International Journal of Microwave and Wireless Technologies

cambridge.org/mrf

Power divider network for dual-fed adaptive antenna

Serafin B. Fischer and Jan Hesselbarth

University of Stuttgart, 70569 Stuttgart, Germany

Research Paper

Cite this article: Fischer SB, Hesselbarth J (2023). Power divider network for dual-fed adaptive antenna. *International Journal of Microwave and Wireless Technologies* **15**, 183–190. https://doi.org/10.1017/S175907872200040X

Received: 10 August 2021
Revised: 2 March 2022
Accepted: 6 March 2022
First published online: 29 March 2022

Key words:
Adaptive antenna; impedance matching; power divider

Author for correspondence:
Serafin B. Fischer,
E-mail: mail@ihf.uni-stuttgart.de

Abstract

Exposing the near field of an antenna to varying dielectric environment causes changes of the antenna input impedance and, thus, unwanted feed mismatch. Feeding such an antenna at different points, and selecting an appropriate feed for best match at a given scenario, may solve the problem. For the case of two scenarios of different dielectric environments and an antenna with two feed points, this work presents a passive power divider network, which keeps the antenna matched to the source in either scenario. Specific impedance transformations in the two branches of the divider network realize power transfer in a first scenario from the source to complex feed impedance at the first antenna feed, while in a second scenario, with now different antenna feed impedances, matched power transfer is from the source to the second antenna feed. Analytical formulae are derived for the design of the divider network. An experiment uses an example antenna with two feeds and a microstrip divider network, connected to a common 50 ohm port. Measurements are conducted with the antenna radiating, first, in air and, secondly, into butter. The measurements show antenna match at 1 GHz in either case and agree well with the analytical results.

Introduction

Nowadays, radio-frequency identification (RFID) techniques are ubiquitous in our daily life, such as in logistics, contactless payment, and medicine. The generic RFID system comprises a mobile device or "tag" and a "reader". While the "reader" can be positioned in a well-defined environment, the "tag" may be exposed to different environments, for example, different dielectric or metallic properties of materials close to the "tag" antenna. These properties may affect and deteriorate the antenna performance significantly.

An illustrative example is a subcutaneous capsule that generates biomedical data, which are then transmitted, by means of an antenna, to an off-body located "reader". Depending on the disposition, the dielectric and conductive properties of the antenna environment vary (different composition of skin, muscles, bones, etc.), which results in an input impedance variation of the antenna, mismatch, and finally, reduced communication range. This variation can be compensated by a tunable matching network with adaptive control [1]. Another possible solution is shown in [2], where high-permittivity dielectric cover, which reduces feed impedance variation, encloses the antenna. Quite similarly, a spacer can increase the distance between antenna and body environment, thereby stabilizing feed impedance [3]. Alternatively, matching can be ensured, while environment of the antenna changes, by selecting a suitable feed of a multiply-fed antenna [4]. Such selection can be obtained by switching. Yet another method uses the combination of different radiating resonance modes of the antenna for different environment scenarios, as proposed in [5] for the respective scenarios of a metal surface close by the antenna and the antenna in the air.

This work considers an antenna with two feed points, represented by two complex feed impedances. A passive and lossless power divider connects a source to the two antenna feeds (Fig. 1). Now considering two scenarios for the environment of the antenna, the pair of complex feed impedances is largely different for either scenario. The power divider consists of two arms. Each arm provides an impedance transformation, which can be realized, for example, by a transmission line structure. Each arm realizes two transformations according to the two scenarios: In one case, it provides conjugate matching toward the source, while for the other scenario, it transforms the corresponding load impedance into the highest possible impedance. Next, the two arms connect to form a power divider fed by the source. As a result, in one scenario, maximum power is transferred to the first antenna feed, while in the second scenario, maximum power goes to the second antenna feed. In both cases, the overall one-port system is matched to a source impedance of, for example, 50 ohm. In the following, a design procedure for the power divider, based on analytical formulas, is presented.

Said operation of the proposed power divider distinguishes it from Wilkinson's divider [6] and its extension for complex load impedances as reported in [7]. Likewise, it is not just a power divider that splits the power unequally, as shown in works [8] and [9]. Rather, the

© The Author(s), 2022. Published by Cambridge University Press in association with the European Microwave Association. This is an Open Access article, distributed under the terms of the Creative Commons Attribution licence (https://creativecommons.org/licenses/by/4.0/), which permits unrestricted re-use, distribution, and reproduction in any medium, provided the original work is properly cited.

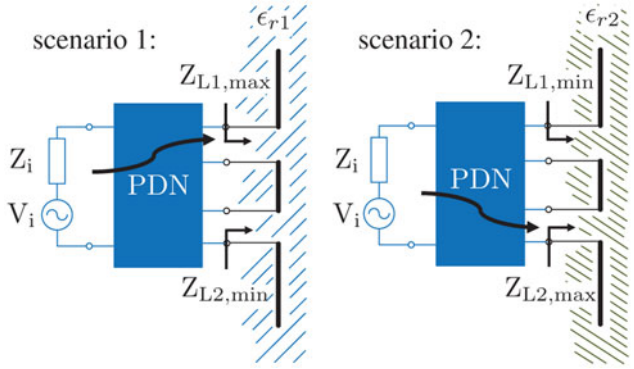


Fig. 1. Concept of matching a dual-fed antenna to a source by a power divider network (PDN). Varying antenna feed impedances due to environmental (near-field) changes to the antenna cause the power flow to change from connecting feed one with the source in the first scenario, while connecting feed two with the source in the second scenario.

proposed power divider concept realizes a particular case of unequal power split, with different splits for two respective sets of complex load impedances at its output ports (i.e. four different, freely-chosen output load impedances). It is optimally adapted to the use case of a dual-fed antenna operating in varying electromagnetic environment.

The proposed technique is fully passive and theoretically lossless, and can be realized in standard transmission line (TL) technology, such as microstrip. Thereby, it is reciprocal, and all statements related to a transmit scenario apply equally to a receiver scenario.

In section "Power divider design", the power divider design is given. It comprises four subsections. In the first one, a most simplified case is presented which shows the principle. In the second subsection, a lumped element-based TL model is introduced, which is the basis for the impedance transformation network (ITN) given in the third subsection. Two of these ITNs form the two branches of the power divider network (PDN), which is discussed in the fourth subsection. Section "Example" shows an example with experimental verification. Two monopoles with unequal lengths, mounted very close to each other, act as a single, dual-fed antenna. They are fed with the PDN. The last section contains the conclusion, consisting of a summary, a classification of this work with regard to RFID technology, and an outlook on future extensions.

Field simulation results are obtained from the finite-element method-based solver in CST Microwave Studio.

Power divider design

Most simplified case

This section explains the principle of this work in a most simplified case. The circuit of Fig. 2, i.e. just two resistors R_1 and R_2, in parallel with source voltage V_i and source resistor R_i, is considered. There are two scenarios assumed, where R_1 and R_2 have different values, while R_i remains constant. For a particular valueset of R_1 and R_2, which is scenario 1, matching between the source, and the two resistors are obtained. In scenario 2 the values of R_1 and R_2 are interchanged in such a way that the source is still matched to the load. In Fig. 3 the normalized (to the maximum available power of the source) power dissipated in R_1 (red dashed line "p_1") and in R_2 (blue dotted line "p_2") are shown. Thereby, the value R_1 varies from 10 to 450 ohm while R_2 varies from

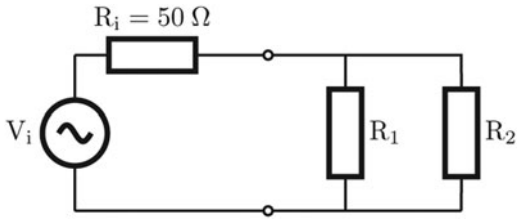


Fig. 2. Two resistors in parallel.

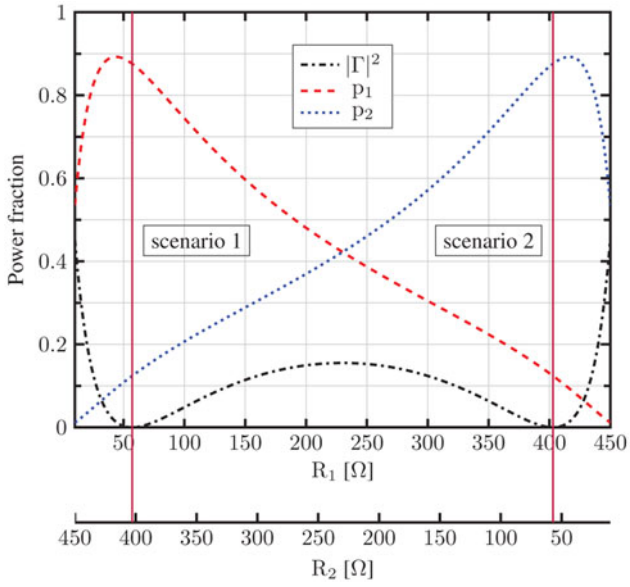


Fig. 3. Portions of the maximum power, which the source can deliver: reflected power $|\Gamma|^2$ (black dash-dotted line), the power dissipated in R_1 (p_1 red dashed line) and the power dissipated in R_2 (p_2 blue dotted line).

450 to 10 ohm as indicated by the two x-axes. The two vertical solid lines indicate the two scenarios. In addition, the reflected power (black dash-dotted line) is plotted. In these scenarios, the reflected power is zero. In scenario 1 the dissipated power in $R_1 = R_{1,\max}$ (≈ 57 ohm) is 87.6 % of the maximum power that the source can deliver. Then, the dissipated power in $R_2 = R_{2,\min}$ (≈ 403 ohm) is 12.4 %. In scenario 2 it is the other way around, as can be seen in Fig. 3. Consequently, this behavior can be seen as a natural power switch that flips in dependency on the load. It is also clear that, for a particular scenario, one of the resistors should have a value that is as close as possible to the value of the source resistance. If this is the case, the value of the other resistor must be very high in order to achieve matching.

In this work, a PDN based on TLs is developed which transforms (for both scenarios) two impedances in such a way that for scenario 1 most of the power is transferred to the first complex impedance and for scenario 2 to the second complex impedance. Therefore, it is important to note that in the general case, the four complex loads can be chosen arbitrarily (contrary to the aforementioned most simplified case).

Transmission line model

TLs shall constitute the power divider. For simplicity, lossless TLs are assumed. The approach is based on the well-known equivalent

https://doi.org/10.1017/S175907872200040X Published online by Cambridge University Press

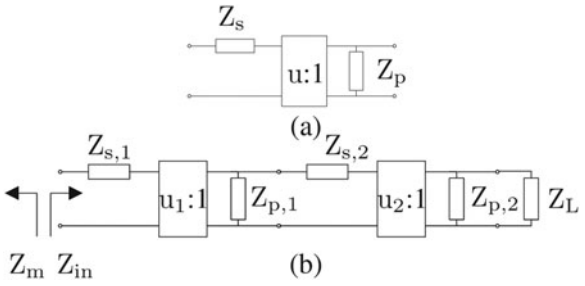


Fig. 4. Lumped-element equivalent circuit model. (a) Circuit model of a transmission line. (b) Circuit model of a two-step transmission line-based impedance transformer.

circuit for a TL as given in [10]. This lumped-element equivalent circuit of a small length of a TL is continued periodically leading again to a lumped-element equivalent circuit and is depicted in Fig. 4(a). It is used to derive the design equations. This circuit comprises a series reactance, a transformer and a shunt reactance. It is equivalent to a TL of length L at a given frequency under conditions of (1).

$$Z_s = j\tan(\beta L)Z_0 = jX_s \tag{1a}$$

$$Z_p = -j\cot(\beta L)Z_0 = jX_p \tag{1b}$$

$$\begin{aligned} u &= \operatorname{sgn}\big(\cos(\beta L)\big)\sqrt{1+\tan(\beta L)^2} \\ &= \operatorname{sgn}\big(\cos(\beta L)\big)\sqrt{1-\frac{X_s}{X_p}} \end{aligned} \tag{1c}$$

Here, β denotes the phase constant, u is the transformer's turns ratio and sgn the sign function.

Impedance transformation network

The impedance transformation network is a series circuit of two TLs (Fig. 4(b)). The load impedance Z_L (i.e. antenna feed impedance) can take two different values. It has the following properties: (i) Maximum power transfer through the ITN, with respect to the source impedance Z_m, for the load impedance $Z_L = Z_{L,\max}$. (ii) Minimum power transfer through the ITN, with respect to the source impedance Z_m, for the load impedance $Z_L = Z_{L,\min}$. In the first case, if $Z_L = Z_{L,\max}$, the ITN provides conjugate-complex match

$$Z_{in}|_{Z_L = Z_{L,\max}} = Z_m^* \tag{2}$$

for maximum power transfer. Considering (1) and the circuit of Fig. 4(b), then (2) leads to

$$X_{p,1} = x \tag{3a}$$

$$X_{p,2} = y \tag{3b}$$

$$X_{s,1} = \frac{N_1}{xD} \tag{3c}$$

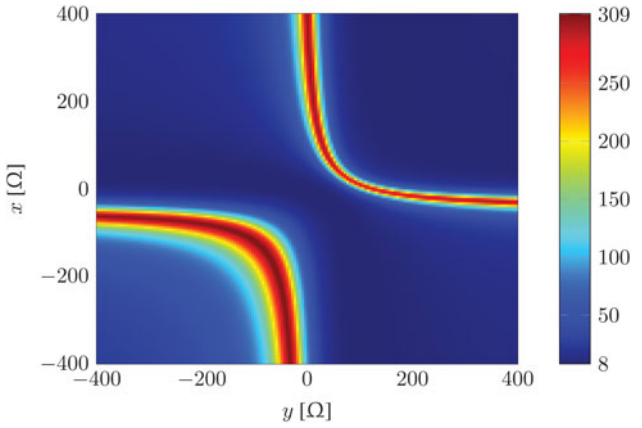


Fig. 5. Colormap of $Re\{Z_{in}|_{Z_L=Z_{L,\min}}\}$ over x and y (see (3)) with $Z_{L,\min} = 20 + j10$ [Ω] and $Z_{L,\max} = 70 - j50$ [Ω] arbitrarily chosen. This map is calculated with (3). Dark red indicates the maximum value while dark blue gives the minimum value in ohm. It should be noted that for $Z_{in}|_{Z_L=Z_{L,\max}}$ (2) is fulfilled for all values of x and y.

$$X_{s,2} = \frac{N_2}{yD} \tag{3d}$$

with

$$\begin{aligned} N_1 = {} & Re\{Z_m - Z_{L,\max}\}x^2y \\ & - 2Im\{Z_m\}Re\{Z_{L,\max}\}xy \\ & - Im\{Z_mZ_{L,\max}^*\}x^2 - Re\{Z_{L,\max}\}|Z_m|^2(x+y) \\ N_2 = {} & Re\{Z_{L,\max} - Z_m\}xy^2 \\ & - 2Im\{Z_{L,\max}\}Re\{Z_m\}xy \\ & + Im\{Z_mZ_{L,\max}^*\}y^2 - Re\{Z_m\}|Z_{L,\max}|^2(x+y) \\ D = {} & Re\{Z_{L,\max}\}x + Re\{Z_m\}y + Im\{Z_mZ_{L,\max}\} \end{aligned}$$

Since (2) leads to two equations (if split in real and imaginary part), but the network itself comprises four parameters, two of them are freely selectable indicated by x and y (with the unit ohm).

It is stated that the input impedance Z_{in} for $Z_L = Z_{L,\min}$ (i.e. $Z_{in}|_{Z_L=Z_{L,\min}}$) must be as high as possible to minimize the power in $Z_{L,\min}$. From here, the real part of Z_{in} is considered only, because the imaginary part will be compensated when two ITNs are combined forming the power divider (see subsection "Power divider network"). Figure 5 colormap shows the real part of Z_{in} if the ITN is terminated in $Z_{L,\min}$ for different values of x and y. Dark red gives the maximum value, whereas dark blue indicates a low value with the unit ohm. Here, example values for $Z_{L,\min}$ and $Z_{L,\max}$ are chosen deliberately. It is calculated with (3) and consequently fulfils (2). To find the maximum values, the following equation must be met

$$\nabla_{x,y}(Re\{Z_{in}|_{Z_L=Z_{L,\min}}\}) = 0. \tag{4}$$

$\nabla_{x,y}$ indicates the gradient with respect to x and y. Both resulting equations are fulfilled for a certain dependency between x and y

https://doi.org/10.1017/S175907872200040X Published online by Cambridge University Press

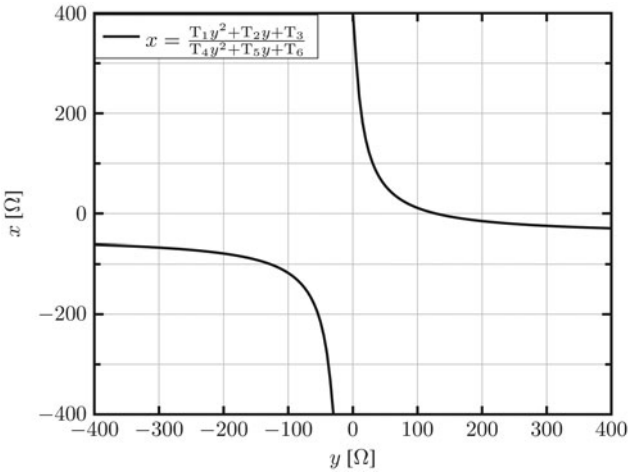


Fig. 6. Plotted function of (5) for $Z_{L,\min} = 20 + j10$ [Ω] and $Z_{L,\max} = 70 - j50$ [Ω]. This curve gives the relation between x and y to obtain the highest possible value of the real part of $Z_{in}|_{Z_L = Z_{L,\min}}$. At the same time (2) for $Z_{in}|_{Z_L = Z_{L,\max}}$ is fulfilled. This curve can be recognized as the maxima of the colormap in Fig. 5.

$$x = \frac{T_1 y^2 + T_2 y + T_3}{T_4 y^2 + T_5 y + T_6} \tag{5}$$

where terms T_i, $i = 1,\ 2,\ \ldots,\ 6$ depend on Z_m, $Z_{L,\max}$, and $Z_{L,\min}$ and are given in Appendix. Inserting (5) into (3) gives the solution that fulfils the aforementioned properties of the ITN. For the same example of Fig. 5 the relation between x and y of (5) is plotted in Fig. 6. The curve can be recognized in Fig. 5 as the maxima. Furthermore, by using (1), the characteristic impedances as well as the electrical lengths of the two TLs, which form the ITN, can be obtained.

Power divider network

Two of the ITN described above form a three-port PDN. As shown in Fig. 7(a), the two scenarios (with source and PDN unchanged) have different loads, Z_{L1} and Z_{L2}. These loads are transformed through the ITNs, and the simplified circuits of Fig. 7(b) are obtained. Here, the subscript "max" indicates the load where the dissipated power is maximized, and the subscript "min" indicates the load where the dissipated power is minimized. For example, $Z_{in,\max}$ denotes the input impedance of the ITN connected to the load $Z_L = Z_{L,\max}$ for the scenario where the maximum power should be delivered to this load. From the circuits of Fig. 7(b), conjugate-complex match to the source impedance Z_i gives

$$Z_i^* = \frac{Z_{in1,\max} Z_{in2,\min}}{Z_{in1,\max} + Z_{in2,\min}} \tag{6a}$$

$$Z_i^* = \frac{Z_{in1,\min} Z_{in2,\max}}{Z_{in1,\min} + Z_{in2,\max}} \tag{6b}$$

which can be written as

$$Z_{in1,\max} = Z_{m1}^* = \frac{Z_i^* Z_{in2,\min}}{Z_{in2,\min} - Z_i^*} \tag{7a}$$

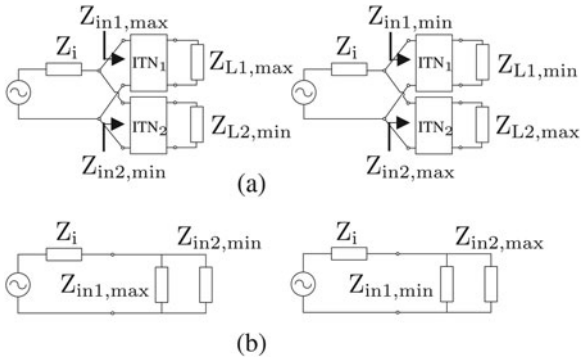


Fig. 7. The scheme of the power divider network (PDN). (a) An illustration of the PDN comprising two impedance transformation networks (ITN) in parallel with its two scenarios. (b) The equivalent circuit of the PDN with its two scenarios.

$$Z_{in2,\max} = Z_{m2}^* = \frac{Z_i^* Z_{in1,\min}}{Z_{in1,\min} - Z_i^*} \tag{7b}$$

The two equations of (7) have unknowns $Z_{in1,\max}$, $Z_{in2,\max}$, $Z_{in1,\min}$, $Z_{in2,\min}$. In addition, (2) and (4) relate $Z_{in,\max}$ and $Z_{in,\min}$ for each of the two ITNs. Therefore, this system of equations can be solved numerically and parameters of the TLs can be calculated.

The PDN presented here is a way of solving the problem of two different environments around an antenna. Intuitively, an alternative approach would be to use only one feed point of the antenna which is then matched with only one ITN for two load impedances (two different environments). However, the design of such a network is not straightforward due to the impedance matching domain problem as discussed in [11] for LC ladder networks. Thus, this single-feed approach is not suitable for a generalized case. On the other hand, the proposed dual-fed approach is straightforward, as shown in the following example.

Example

The procedure developed in section "Power divider design" is applied to a practical example of an adaptive antenna. The idea is to use the PDN to feed two monopoles (diameter of 2 mm) of different length, very close to each other ($\approx \lambda/15$) at 1 GHz (Fig. 8(a)). Here, "M1" indicates monopole 1 (length 72 mm $\approx \lambda/4$) and "M2" monopole 2 (length 35 mm $\approx 0.116\lambda$). In the first scenario, the monopoles are placed in free space. In the second scenario, the monopoles are fully immersed in a lossy organic material (namely, butter). This example setup of the two coupled monopole antenna was chosen because it allows for an easy and clear separation of the electromagnetic environment of the antenna (namely, "air" versus "butter") from the PDN (the microstrip circuit in the opposite side of the antenna ground plane). The PDN matches the monopoles, in both scenarios, to a single 50 ohm source. From inspection of field simulation field plots, it can be noted that in the first scenario (free space), most of the power is radiated via the first monopole, while in the second scenario (butter), mostly the second monopole radiates.

The dielectric properties of butter are measured. Transmission through a cylindrical cavity resonator, at first air-filled and then filled with butter (Fig. 8(b)), is measured and modeled in a field

https://doi.org/10.1017/S175907872200040X Published online by Cambridge University Press

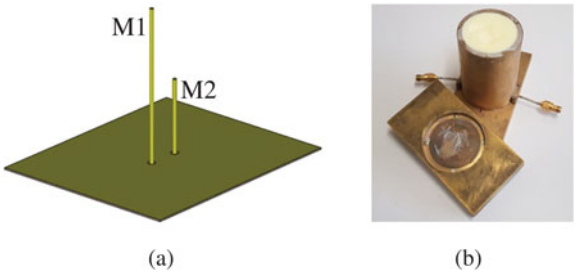


Fig. 8. (a) Two monopoles of different length next to each other forming the dual-fed adaptive antenna. (b) Photo of the butter-filled cylindrical resonator (opened for clarity) for determination of the material properties of butter.

Table 1. Simulated input impedances of the monopoles

Scenario 1	Free-space	
Notation	$Z_{L1,\max}$ [Ω]	$Z_{L2,\min}$[Ω]
1st simulation	24.1 + *j*1.2	2.6 − *j*113
converged	25 + *j*1.7	− 35.5 − j162.1
Scenario 2	Butter	
Notation	$Z_{L1,\min}$ [Ω]	$Z_{L2,\max}$[Ω]
1st simulation	56.9 − j102.1	12.3 + *j*8.9
converged	− 33.4 − j53.6	14.9 + j8.4

simulator, allowing to obtain permittivity and loss tangent by fitting. Permittivity $\varepsilon_{r,butter} = 4.13$ and $\tan\delta_{butter} = 0.04$ is found at 1 GHz.

Field simulation provides the respective input impedances for the two monopoles M1, M2 for the two scenarios, as listed in Table 1 under notation "1st simulation". The indices are chosen such that M1 is primarily fed to radiate in the free-space scenario, whereas M2 is primarily fed to radiate in the "butter scenario". For illustration, Fig. 9 shows plots of the variation of the monopole input impedances while linearly varying permittivity and loss tangent from the values of the first scenario to their values of the second scenario. It should be noted that strong coupling between the two monopoles (also expected for most dual-fed antenna structures) leads to some change of feed impedance of one monopole while the other monopole's feed is connected to a varying load (active impedance). The PDN is derived from the impedances, which in turn are obtained from a field simulation assuming simple, e.g. 50 ohm, port impedance. This PDN, however, then provides different impedances to the antenna, changing the active impedances of the antenna network at its ports. In an iterative procedure, these updated antenna impedances allow to derive an updated PDN. This process converges quickly. Note that additional field simulations are not required, as the scattering parameter matrix (or impedance matrix) of the antenna (for each scenario) needs to be obtained only at the beginning.

Table 1 lists under notation "converged" the respective input impedances of the two monopoles M1, M2 for the two scenarios. Using the input impedances of Table 1, equations (1)–(7) permit the calculation of impedances and electrical lengths of the TLs forming the ITNs (Fig. 10, Table 2). These calculations are executed with Matlab. For each ITN, a remaining degree of freedom allows to select one parameter. In this example, the parameter

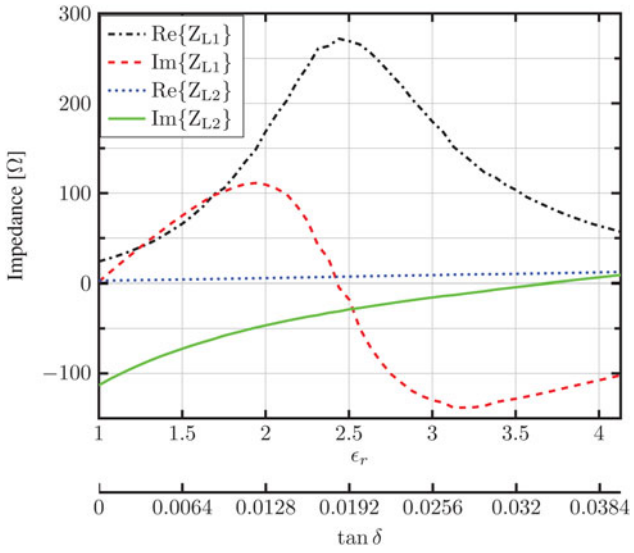


Fig. 9. Simulated input impedance of the two monopoles when assuming a linear transition of the relative permittivity and loss tangent from the scenario with air to the one with butter. It holds $Z_{L1}(\varepsilon_r = 1,\ \tan\delta = 0) = Z_{L1,\max}$, $Z_{L2}(1,\ 0) = Z_{L1,\min}$, $Z_{L1}(4.13,\ 0.04) = Z_{L1,\min}$, and $Z_{L2}(4.13,\ 0.04) = Z_{L2,\max}$.

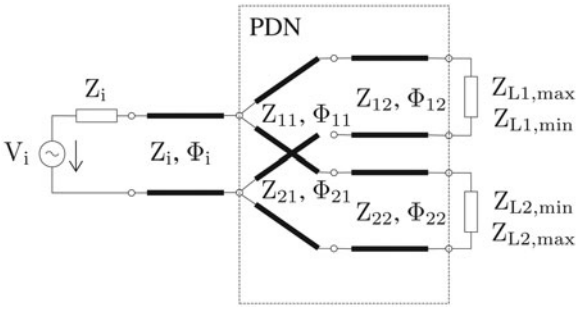


Fig. 10. Equivalent circuit of the PDN.

$y = -5$ ohm is chosen for each ITN (this choice is governed by the resulting, "realizable" TL impedances).

Table 2 lists the obtained parameters of the TLs of the PDN. The values for the PDN of the first iteration (notation "1st simulation") do not differ much from the values obtained from the converged iterative design process (notation "converged"). In particular, in a practical realization of the PDN in microstrip technology, the differences will be negligible. However, for an even-stronger coupling between the ports of the dual-fed antenna, the changes during the iterative design procedure may become larger.

In Fig. 11 the simulated (here, TLs are lossless) portions of the maximum power that can be delivered from the source of the reflected power $|\Gamma|^2$ (black dash-dotted line), the power dissipated in $Re\{Z_{L1}\}$ (p_1 red dashed line), and the dissipated power in $Re\{Z_{L2}\}$ (p_2 blue dotted line) are plotted. Thereby, the input impedance changes over the relative permittivity and the loss tagent is considered (see Fig. 9). In the air-scenario, 99.8% of the maximum power is consumed by monopole M1, while only 0.2% is dissipated in monopole M2. If the monopoles are exposed in butter, the reflected power is about 0.2%, the power in M1 is 9.5 %, and in M2 is 90.3%.

https://doi.org/10.1017/S175907872200040X Published online by Cambridge University Press

Table 2. Characteristic impedances and electrical lengths of the PDN transmission lines for $y = -5\ \Omega$

Z_{11}	Z_{12}	Z_{21}	Z_{22}	Φ_{11}	Φ_{12}	Φ_{21}	Φ_{22}
1st simulation							
[Ω]				[°]			
41.3	28.5	125.8	58	88.4	80	79.3	85
Converged							
[Ω]				[Ω]			
46.7	33.3	96.9	56.5	77.8	81.5	82.0	84.8

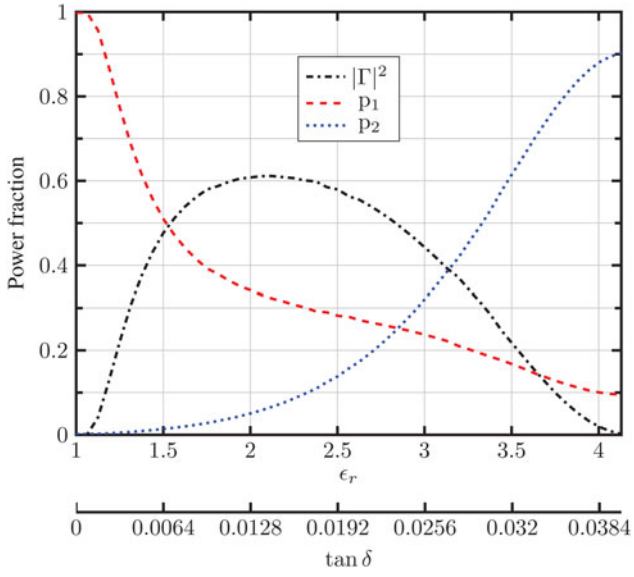


Fig. 11. Simulated portions of the maximum power of the reflected power $|\Gamma|^2$ (black dash-dotted line), the power dissipated in $Re\{Z_{L1}\}$ (p_1, red dashed line) and dissipated power in $Re\{Z_{L2}\}$ (p_2, blue dotted line) over different valuesets of the relative permittivity and the loss tangent. In the scenario where the monopoles are placed in air ($\varepsilon_r = 1$, $\tan\delta = 0$) the reflected power is zero and the dissipated power p_1 in $Re\{Z_{L1}\}$ is about 99.8% of the maximum power that can be delivered from the source. Then the power p_2 in $Re\{Z_{L2}\}$ is 0.2%. In the scenario of butter ($\varepsilon_r = 4.13$, $\tan\delta = 0.04$) $|\Gamma|^2$ is 0.2%, p_1 is 90.3%, and p_2 is 9.5%.

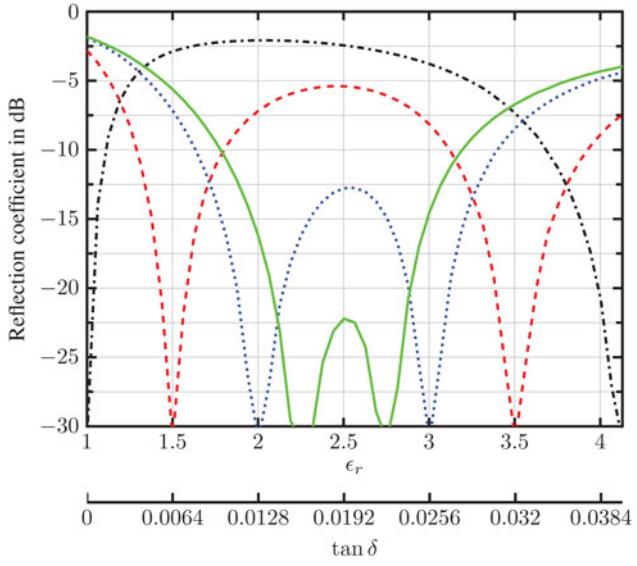


Fig. 12. Simulated reflection coefficient $|\Gamma|$ in dB for the two-monopole-antenna with four different PDNs, corresponding to four pairs of environmental scenarios to the antenna. Case (i): $\varepsilon_r = \{1,\ 4.13\}$ in black dash-dotted line. Case (ii): $\varepsilon_r = \{1.5,\ 3.5\}$ in red dashed line. Case (iii): $\varepsilon_r = \{2,\ 3\}$ in blue dotted line. Case (iv): $\varepsilon_r = \{2.25,\ 2.75\}$ in green solid line. The associated loss tangent ($\tan\delta$) values are scaled proportionally.

So far, optimum operation was required at two different scenarios, as illustrated in Fig. 11, showing the reflected power at source becoming zero for $\varepsilon_r = 1$ and $\varepsilon_r = 4.13$. A modification of the use-case may require good performance (i.e. small reflected power) over a range of dielectric property of the electromagnetic environment. Such use-case may represent somewhat varying material property and/or varying geometry of the environment of the antenna, as it can be expected for many RFID-like applications.

Exposing the pair of coupled monopole radiators to three other pairs of environmental dielectric scenarios, Fig. 12 illustrates the simulated resulting reflection coefficient magnitude. The four permittivity-pairs related to Fig. 12 are: (i) $\varepsilon_r = \{1,\ 4.13\}$, (ii) $\varepsilon_r = \{1.5,\ 3.5\}$, (iii) $\varepsilon_r = \{2,\ 3\}$, (iv) $\varepsilon_r = \{2.25,\ 2.75\}$. Obviously, the dielectric property of the electromagnetic environment can always vary by a small amount, without resulting in large mismatch. Once the two "optimally matched" permittivity values are close-enough to each other (as in cases (iii) and (iv)), a range of electromagnetic environment, leading well-matched input impedance, is obtained. Similar behavior is common to any ITN.

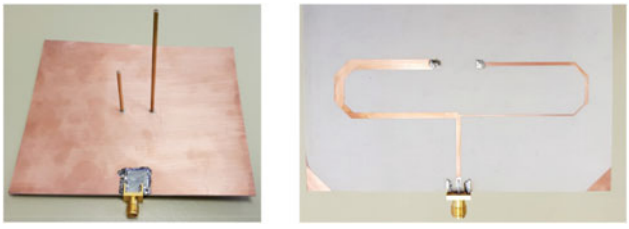


Fig. 13. Adaptive antenna prototype. Left: two monopoles over board ground. Right: microstrip PDN and feed.

The microstrip line parameters are readily found for the circuit realized on Rogers RT6002 substrate (thickness 0.762 mm, $\varepsilon_{rel} = 2.94$, $\tan\delta = 0.0012$). Figure 13 shows the realization of the two monopole radiators and the PDN on a microstrip circuit board. The ground layer has openings of 4 mm diameter for the monopoles. The monopole metal rods pass through the board and are soldered to the microstrip traces. The feed reflection magnitude at the coax connector, measured for the two scenarios, is shown in

https://doi.org/10.1017/S175907872200040X Published online by Cambridge University Press

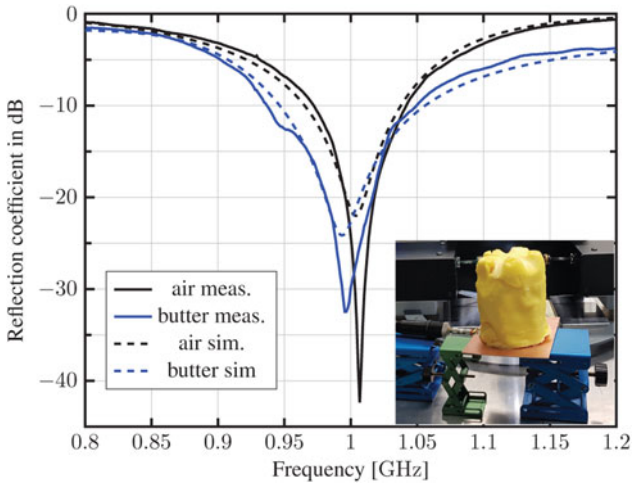


Fig. 14. Measured and simulated reflection coefficient of the adaptive antenna for both scenarios (air and butter). The inset picture shows the measurement setup for the scenario with butter.

Fig. 14. Good match is achieved for both scenarios (free-space and butter). Furthermore, the measured curves are in good agreement with the field simulations.

Conclusion

Analytical formulae for a power divider feed network for a dual-fed antenna are presented. If the antenna operates in two electromagnetically different environments, called scenarios, its feed impedances will change. The proposed power divider feed network directs the power from a matched source to the first antenna feed in the first scenario, and to the second antenna feed in the second scenario. The proposed power divider feed network is passive and assumed lossless. In a practical demonstration, two strongly coupled monopole radiators of largely different length are fed by an accordingly designed power divider feed network. This structure radiates with perfect source match (50 ohm) into free space, but also when completely immersed into butter ($\varepsilon_{r,\,butter} = 4.13$, $\tan\delta_{butter} = 0.04$). The measurements confirm the derived theoretical formulae.

The presented PDN can be used with RFID tags to adapt the antenna to two different environments. It ensures an energy-efficient operation of the RFID tag without much power being reflected at the antenna input.

From a theoretical point of view, the number of different environmental scenarios, as well as the number of antenna feed points, can both be increased to a number larger than two. If N scenarios shall be covered with an antenna having N feed points, then the extension of the approach discussed in this paper (here $N = 2$) shows that each of the N arms of the power divider requires N sections of TL to realize the appropriate impedance transformation. However, already for $N = 3$, these nine lines contribute to loss and increase the physical size of the circuit likely beyond a practical limit.

Acknowledgments. This work was supported in part by the German Research Foundation (DFG) under grant HE6429/7-2.

References

1. **Gu Q and Morris AS** (2013) A new method for matching network adaptive control. *IEEE Transactions on Microwave Theory and Techniques* **61**, 587–595.
2. **Nikolayev D, Zhadobov M, Karban P and Sauleau R** (2016) Increasing the radiation efficiency and matching stability of in-body capsule antennas, 10th European Conference on Antennas and Propagation (EuCAP), Davos, pp. 1–5.
3. **Dissanayake T, Esselle KP and Yuc MR** (2009) Dielectric loaded impedance matching for wideband implanted antennas. *IEEE Transactions on Microwave Theory and Techniques* **57**, 2480–2487.
4. **Rasteh M and Hesselbarth J** (2018) Dipole antenna with multiple feeds adapting to the environment, IEEE Asia-Pacific Conference on Antennas and Propagation (APCAP), Auckland, pp. 38–41.
5. **Fischer SB and Hesselbarth J** (2020) A single-layer planar antenna unaffected by a possibly close-by metal surface, 14th European Conference on Antennas and Propagation (EuCAP), Copenhagen, Denmark, pp. 1–5.
6. **Wilkinson EJ** (1960) An N-way hybrid power divider. *IRE Transactions on Microwave Theory and Techniques* **8**, 116–118.
7. **Rosloniec S** (1996) Three-port hybrid power dividers terminated in complex frequency-dependent impedances. *IEEE Transactions on Microwave Theory and Techniques* **44**, 1490–1493.
8. **Li J and Wang B** (2011) Novel design of Wilkinson power dividers with arbitrary power division ratios. *IEEE Transactions on Industrial Electronics* **58**, 2541–2546.
9. **Lim J-S, Lee S-W, Kim C-S, Park J-S, Ahn D and Nam S** (2001) A 4:1 unequal Wilkinson power divider. *IEEE Microwave and Wireless Components Letters* **11**, 124–126.
10. **Pozar DM** (2011) *Microwave Engineering*, 4th Ed. New York: Wiley.
11. **Sun Y and Fidler JK** (1996) Determination of the impedance matching domain of passive LC ladder networks: theory and implementation. *Journal of the Franklin Institute* **333**, 141–155.

Appendix

Six coefficients T_i, $i = 1,\ 2,\ \ldots,\ 6$ appear in (5). Their explicit expression read:

$$\begin{aligned} T_1 = {} & Re\{Z_m\}\big(Re\{Z_{L,\min}\}^2 - Re\{Z_{L,\max}\}^2 \\ & + \big(Im\{Z_{L,\min}\} - Im\{Z_{L,\max}\}\big)^2 + \sqrt{A}\big) \\ & + 2Im\{Z_m\}Re\{Z_{L,\max}\}\big(Im\{Z_{L,\min}\} \\ & - Im\{Z_{L,\max}\}\big) \end{aligned} \tag{A.1}$$

$$\begin{aligned} T_2 = {} & 2|Z_{L,\max}|^2\big(Im\{Z_{L,\max}Z_m^*\} \\ & - 2Re\{Z_m\}Im\{Z_{L,\min}\}\big) \\ & + 2|Z_{L,\min}|^2 Im\{Z_m Z_{L,\max}\} \\ & + 2Im\{Z_{L,\max}\}Re\{Z_m\}\sqrt{A} \end{aligned} \tag{A.2}$$

$$\begin{aligned} T_3 = {} & Re\{Z_m\}|Z_{L,\max}|^4 \\ & - Re\{Z_m\}Re\{Z_{L,\max}^2\}|Z_{L,\min}|^2 \\ & + Re\{Z_m\}\sqrt{A}|Z_{L,\max}|^2 \\ & - 2Re\{Z_m\}Im\{Z_{L,\min}\}Im\{Z_{L,\max}\}|Z_{L,\max}|^2 \\ & - 2Im\{Z_m\}Re\{Z_{L,\max}\}\big(Im\{Z_{L,\min}\}|Z_{L,\max}|^2 \\ & - Im\{Z_{L,\max}\}|Z_{L,\min}|^2\big) \end{aligned} \tag{A.3}$$

$$T_4 = 2Re\{Z_{L,\max}\}\big(Im\{Z_{L,\max}\} - Im\{Z_{L,\min}\}\big) \tag{A.4}$$

$$T_5 = 2Re\{Z_{L,\max}\}\big(|Z_{L,\max}|^2 - |Z_{L,\min}|^2\big) \tag{A.5}$$

$$\begin{aligned} T_6 = {} & 2Re\{Z_{L,\max}\}\big(Im\{Z_{L,\min}\}|Z_{L,\max}|^2 \\ & - Im\{Z_{L,\max}\}|Z_{L,\min}|^2\big) \end{aligned} \tag{A.6}$$

with

$$\begin{aligned} A = {} & \big(Im\{Z_{L,\min}\} - Im\{Z_{L,\max}\}\big)^4 \\ & + \big(Re\{Z_{L,\min}\}^2 - Re\{Z_{L,\max}\}^2\big)^2 + 2\big(Re\{Z_{L,\min}\}^2 \\ & + Re\{Z_{L,\max}\}^2\big)\big(Im\{Z_{L,\min}\} - Im\{Z_{L,\max}\}\big)^2 \end{aligned}$$

https://doi.org/10.1017/S175907872200040X Published online by Cambridge University Press



Serafin B. Fischer was born in Buchholz in der Nordheide, Germany, in 1991. He received the B.Sc. and M.Sc. degrees in electrical engineering from the University of Stuttgart, Germany in 2016 and 2018, respectively. He is currently pursuing the Ph.D. degree at the University of Stuttgart, Stuttgart, Germany. His current research interests include matching networks, adaptive antennas, and antenna-arrays.



Jan Hesselbarth (A'96–M'04) was born in Dresden, Germany, in 1970. He received the Ph.D. degree from the Swiss Federal Institute of Technology (ETH), Zurich, Switzerland, in 2002. From 2001 to 2005, he was a Design Engineer with Huber +Suhner, Pfaffikon, Switzerland. From 2005 to 2008, he was a Technical Staff Member with Bell Laboratories, Dublin, Ireland. He was a Senior Researcher and Lecturer with ETH Zurich. Since 2011, he has been a Professor with the Institute of Radio Frequency Technology, University of Stuttgart, Stuttgart, Germany. His current research interests include antennas and millimeter-wave circuits and packaging.

https://doi.org/10.1017/S175907872200040X Published online by Cambridge University Press